A&A 395, 305–320 (2002)
DOI: 10.1051/0004-6361:20021349
© ESO 2002

Astronomy & Astrophysics

Hanle effect with angle-dependent partial redistribution

K. N. Nagendra[1,2], H. Frisch[2], and M. Faurobert[2]

[1] Indian Institute of Astrophysics, Sarjapur Road, Koramangala Layout, Bangalore 560 034, India
[2] Laboratoire G. D. Cassini (CNRS, UMR 6529), Observatoire de la Côte d'Azur, BP 4229, 06304 Nice Cedex 4, France

Received 2 May 2002 / Accepted 9 July 2002

Abstract. The polarized line transfer equation for the Hanle effect is solved in the framework of an exact partial frequency redistribution (PRD) theory developed by Bommier (1997a,b). In that theory the effect of collisions on the Hanle effect is considered self-consistently. We follow that approach in the line transfer computations presented here. The theory formulated by Bommier clearly recognizes two levels of approximations for exact PRD, in order to facilitate the solution of the line transfer equation. The second level employs angle-dependent redistribution functions, and numerically represents a more difficult problem compared to the third level, which involves only the use of angle-averaged frequency redistribution functions. We present a method which can solve the problem in both the levels of approximation. The method is based on a perturbative approach to line polarization. Although computationally expensive, it offers the only practical means of solving the angle-dependent Hanle PRD problem. We discuss the numerical aspects of assembling the so called "frequency domain dependent redistribution matrices", and also an efficient way of computing the scattering integral. Some examples are presented to illustrate the interesting aspects of the Hanle-PRD problem with angle-dependent frequency redistribution. A comparison of the emergent profiles computed under angle-averaged and angle-dependent redistribution is carried out, and the effect of collisions is investigated. We show that it is necessary to incorporate an angle-dependent redistribution mechanism especially in the computation of the Stokes U parameter. We demonstrate that the use of simple frequency domains is good enough in practical applications of the Hanle PRD theory.

Key words. line: formation – polarization – scattering – magnetic fields – methods: numerical – Sun: atmosphere

1. Introduction

The study of scattering polarization in spectral lines has become a front line area of research in solar physics (see Stenflo & Nagendra 1996; Nagendra & Stenflo 1999). The mechanism of resonance scattering on bound atomic levels produces polarization of radiation. A modification of this basic process by an external weak magnetic field is called the Hanle effect (see Stenflo 1994; Trujillo Bueno 2001; and Trujillo Bueno et al. 2002 for a description). The magnetic field not only modifies the angular phase matrix but also affects the frequency correlations between incident and scattered photons. During the life time of the excited state, the elastic collisions reduce the angular correlations, causing frequency redistribution and a depolarization of the line radiation. The inelastic collisions, on the other hand, cause transitions between the bound states. The Hanle scattering phenomenon and the intervention of collisions are both treated self-consistently in two pioneering papers by Bommier (1997a,b: henceforth [B97a,b]). Apart from deriving the exact relations for the Hanle scattering redistribution matrix, the author also presented useful limiting approximations to the same, for practical applications. These approximations make use of the possibility to decompose the 2D frequency space (x, x'), with x' the incident frequency, and x the outgoing frequency, into several domains. In each of them, the redistribution matrix which describes the scattering (at the microscopic level), can be written as a sum of factorized terms. Each term involves a scalar redistribution function that multiplies a phase matrix. The so-called Approximation Level-II uses the angle-dependent (AD) version of the redistribution functions, and Approximation Level-III the corresponding angle-averaged (AA) function. The numerical method developed in this paper for solving the transfer problem handles Level-II and also the relatively simpler Level-III approximation.

The work of Omont et al. (1972, 1973), developed within the quantum theory of resonance scattering, marks the beginning of partial frequency redistribution (PRD) line formation theory with Hanle effect. The redistribution matrices describing the scattering of polarized radiation were explicitly calculated much later by Domke & Hubeny (1988) for resonance scattering (the non-magnetic case). The exact theory was later developed in [B97a,b] taking into account the role of magnetic fields, through a quantum electro-dynamical approach. The earlier works of Landi Degl'Innocenti (1983, 1984, 1985) based on the atomic density matrix approach, did not consider frequency redistribution problems. They were introduced, but in

Send offprint requests to: K. N. Nagendra,
e-mail: knn@iiap.ernet.in

Article published by EDP Sciences and available at http://www.aanda.org or http://dx.doi.org/10.1051/0004-6361:20021349

heuristic manner, in Landi Degl'Innocenti et al. (1997). The 2-level atom model is still retained in [B97a,b] for the sake of simplicity. Recently Bommier & Stenflo (1999) have derived a redistribution matrix for the combined Hanle-Zeeman scattering problem, based on a semi-classical approach. It provides a clear physical picture of the results obtained in [B97a,b].

In two papers published earlier on this subject, we have drawn attention to the importance of taking into account the coupling between frequency and angular redistribution which is present in the exact formulation of Hanle effect derived in [B97b] and remains in the Level-II approximation which involves the AD redistribution function. In Frisch et al. (2001), analytical arguments are presented to show that this coupling leads to non-zero Stokes U in the symmetric case of a magnetic field perpendicular to the slab (contrary to the normal expectations!). It is also shown that the frequency-integrated Stokes U does vanish. The same conclusions are substantiated in another paper through some numerical computations (see Faurobert et al. 2002).

In the present paper, we elaborate on this question, and further discuss several aspects of the Hanle redistribution problem, using angle-averaged, and angle-dependent functions. In a recent paper Fluri et al. (2002) have proposed a generalized PALI (Polarized Approximate Lambda Iteration) method for the Hanle effect under Approximation Level-III. It handles the AA frequency redistribution case with the frequency domain decomposition introduced in [B97b]. It is very fast because, like the PALI methods developed earlier (see Nagendra et al. 1998, 1999), it makes use of the azimuthal Fourier decomposition of the Hanle phase matrix and Stokes vector. A generalization of this method to the AD frequency redistribution case has yet to be developed. Here we use a perturbative approach. It is simple and direct, but requires large memory and is computationally very slow, because directions have to be described by their azimuthal and polar angles. In the PALI method, only polar angles have to be considered. Thus we can state that the emphasis in this paper is more on exploring the physical aspects of this complex problem, than on proposing the perturbative approach as a practical method. A review of the numerical methods for the solution of polarized line transfer equations can be found in Nagendra (2002). A brief assessment of the generalized PALI method as well as the perturbative method is presented in Nagendra & Frisch (2002).

In Sect. 2 and in the Appendix, we present the required equations. We highlight the peculiarities of the angle-dependent PRD problem for the Hanle effect, and the structure of frequency domains. We also briefly discuss the angle-averaged Approximation (Level-III). In Sect. 3 we describe the method of solution and mention the numerical aspects. In Sect. 4 we present some physical results through illustrative examples.

2. The basic equations

In this section we present the basic equations of the general Hanle effect polarized line transfer problem.

2.1. The polarized line radiative transfer equation

The one-dimensional line transfer equation for polarized Hanle scattering problem may be written as:

$$\mu \frac{\partial \boldsymbol{I}(\tau, x, \boldsymbol{n})}{\partial \tau} = [\phi(\tau, x) + \beta(\tau)]\,[\boldsymbol{I}(\tau, x, \boldsymbol{n}) - \boldsymbol{\mathcal{S}}(\tau, x, \boldsymbol{n})]\,, \qquad (1)$$

where $\boldsymbol{I} = (I, Q, U)^{\mathrm{T}}$ represents the Stokes vector. In the restricted problem of pure Hanle effect, we do not need to consider the V Stokes parameter, since it gets completely decoupled from the other three parameters. Unless stated otherwise, all the physical quantities and symbols in this paper have the same meaning as in Nagendra et al. (1998, 1999), and Fluri et al. (2002). The Stokes source vector may be written as

$$\boldsymbol{\mathcal{S}}(\tau, x, \boldsymbol{n}) = \frac{\phi(\tau, x)\boldsymbol{\mathcal{S}}_\ell(\tau, x, \boldsymbol{n}) + \beta(\tau)\boldsymbol{\mathcal{B}}_{\mathrm{th}}(\tau)}{\phi(\tau, x) + \beta(\tau)}\,, \qquad (2)$$

where $\boldsymbol{\mathcal{B}}_{\mathrm{th}}(\tau) = (B_{\nu_0}, 0, 0)^{\mathrm{T}}$ with B_{ν_0} being the unpolarized thermal source vector (Planck function). The polarized line source vector $\boldsymbol{\mathcal{S}}_\ell$ may be written as

$$\boldsymbol{\mathcal{S}}_\ell(\tau, x, \boldsymbol{n}) = \varepsilon \boldsymbol{\mathcal{B}}_{\mathrm{th}}(\tau) + \frac{1}{\phi(\tau, x)} \times \int_{-\infty}^{+\infty} \mathrm{d}x' \oint \frac{\mathrm{d}\Omega'}{4\pi} \hat{\mathcal{R}}(x, x'; \boldsymbol{n}, \boldsymbol{n}'; \boldsymbol{B})\, \boldsymbol{I}(\tau, x', \boldsymbol{n}')\,, \qquad (3)$$

where the thermalization parameter ε represents the probability that a photon is destroyed by collisional de-excitation. The usual single scattering albedo $(1 - \varepsilon)$ is absorbed into the definition of the redistribution matrix $\hat{\mathcal{R}}$.

In the non-magnetic case, the redistribution matrix can be written as the sum of terms, each one being the product of a frequency-dependent redistribution function and a polarization phase matrix (see Domke & Hubeny 1988, and [B97a]). In the presence of an external magnetic field, frequency redistribution and polarization are coupled together. However, in the limit of weak magnetic fields, i.e. for the Hanle effect, it is possible to construct approximations to the redistribution matrix in which polarization and frequency redistribution are decoupled. Investigating the 90° scattering of a pencil of radiation with the exact redistribution matrix, Bommier [B97b] has observed well-defined frequency domains where (Q/I) and (U/I) take constant values (see Fig. 2 of [B97b], upper panels). This behavior is consistent with the idea that in each domain the redistribution matrix can be factorized into the product of a phase matrix and a scalar redistribution function. The domains are separated by sharp transition regions which are approximated by step functions. These boundaries correspond to core-wing transitions in the generalized absorption profiles. Since the theory developed in [B97b] incorporates the effect of collisions, the R_{II} and R_{III} type redistribution functions appear in the redistribution matrix. The approximation Level-II involves the AD scalar redistribution functions and the approximation Level-III their angle-averaged versions. Figures 1 and 2 show the frequency domains for the AD case and AA case, respectively. There are three domains associated with R_{III} and two domains associated with R_{II}.

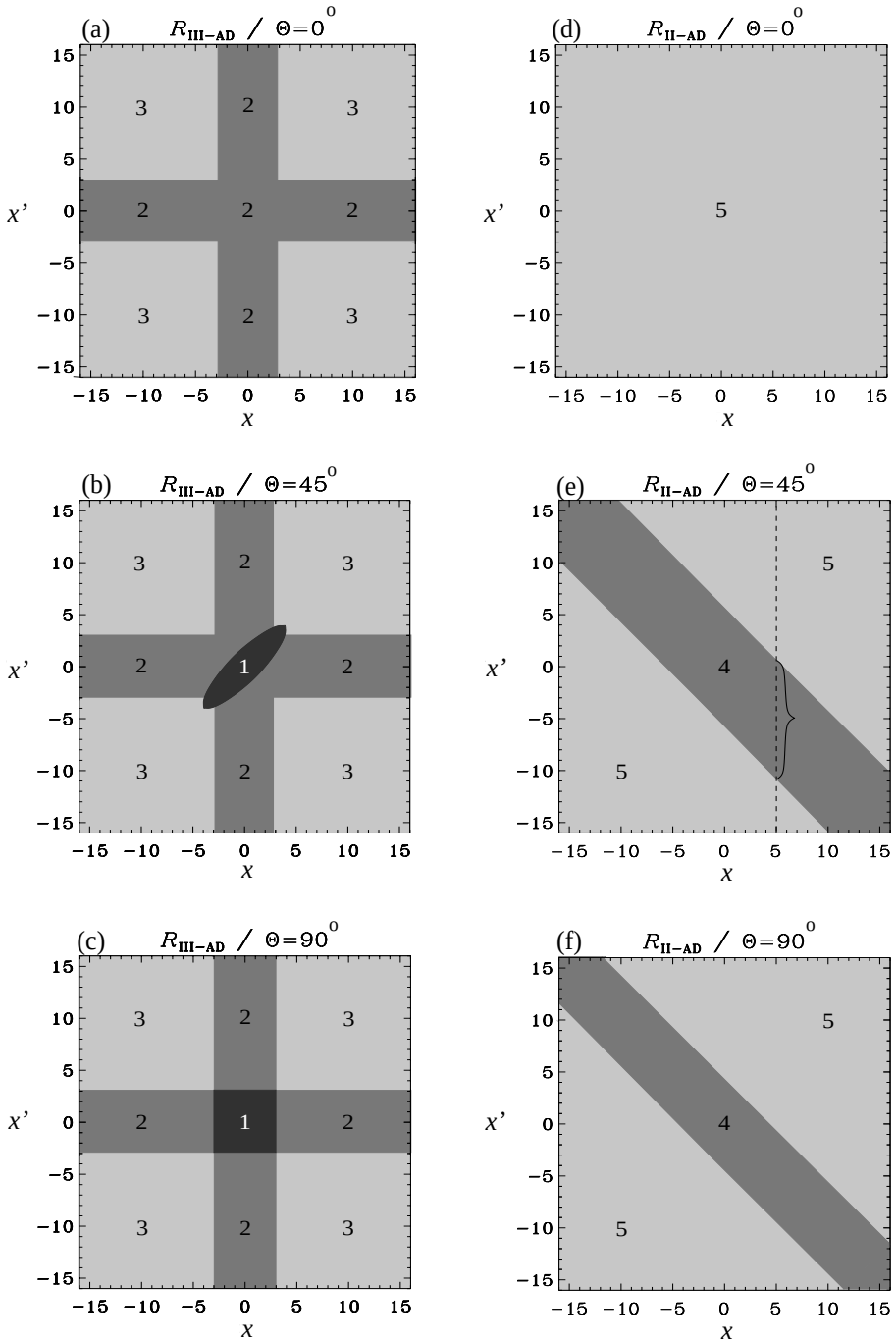

Fig. 1. The frequency domains for solving the angle-dependent Hanle redistribution problem. The panels **a–c)** refer to $R_{\rm III-AD}(x, x', \Theta)$, and the panels **d–f)** refer to $R_{\rm II-AD}(x, x', \Theta)$. The domains marked as 1, 2, 3 refer to $R_{\rm III-AD}$, while those marked as 4, 5, refer to $R_{\rm II-AD}$. In the text they are referred as Dm, $m = 1, 2, 3$ and Dn, $n = 4, 5$. Notice a strong dependence of the domain shape on the scattering angle Θ. The domains are defined in Eqs. (A.1) and (A.2) of the Appendix. The dotted vertical line in Fig. 1e shows the "line of integration" over frequency x', for a given value of x. The damping parameter $a = 10^{-3}$ is used. See the Appendix for more details.

In the Level-II approximation, which handles AD redistribution functions, the line source function may be written as

$$\mathcal{S}_{\ell,\rm AD}(\tau, x, \boldsymbol{n}) = \varepsilon \mathcal{B}_{\rm th}(\tau) + \frac{1}{\phi(\tau, x)} \int_{-\infty}^{+\infty} {\rm d}x' \oint \frac{{\rm d}\Omega'}{4\pi} \times \Big[\hat{P}_{\rm II}(\boldsymbol{n}, \boldsymbol{n}'; {\rm Dn})\, R_{\rm II-AD}(x, x', \Theta) + \hat{P}_{\rm III}(\boldsymbol{n}, \boldsymbol{n}'; {\rm Dm})\, R_{\rm III-AD}(x, x', \Theta)\Big] \mathcal{I}(\tau, x', \boldsymbol{n}'). \quad (4)$$

For each set of frequencies (x, x') is associated a domain Dm for $R_{\rm III}$ and Dn for $R_{\rm II}$. In the AD case, the shape of the domains depend on the scattering angle $\Theta(\boldsymbol{n}, \boldsymbol{n}')$. In the Level-III approximation, which works with AA redistribution functions, the line source function is again given by Eq. (4) with the angle-dependent redistribution functions replaced by their angle-averages. Further the frequency domains do not depend on Θ. The polarization matrices are given in the Appendix Sect. A3

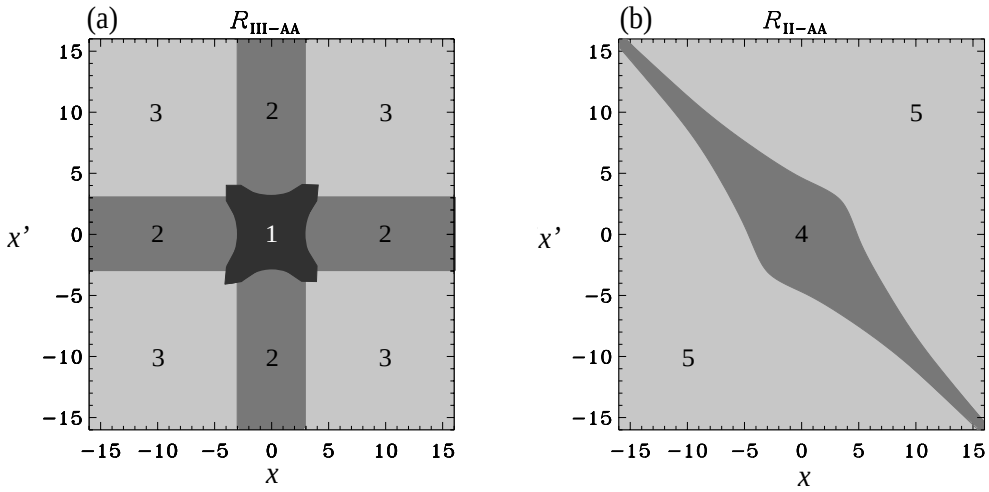

Fig. 2. The frequency domains for solving the angle-averaged (AA) Hanle redistribution problem. Notice the similarity of $R_{\rm III-AA}$ domain with the AD domain $R_{\rm III-AD}(x, x', \Theta = 90°)$ in Fig. 1. Notice also the narrowing of the diagonal stripe in the case of $R_{\rm II-AA}$, for large frequencies, which indicates the diminished role of Hanle effect in the line wings. A damping parameter $a = 10^{-3}$ is used. See Appendix Sect. A.2 for more details.

(Eqs. (A.8) to (A.12)). For a given domain Dm or Dn, they have the same expression in the AD and AA cases, but the shapes of the domains depend on Θ in the AD case.

2.2. The frequency domains

We now discuss the frequency domains shown in Fig. 1. Forward scattering ($\Theta = 0°$) is a very special case. Domain-1 (for $R_{\rm III-AD}$) and Domain-4 (for $R_{\rm II-AD}$) do not exist because the conditions in Eqs. (A.1) and (A.2) cannot be satisfied.

We first consider the case of $R_{\rm II-AD}$. Domain-5 represents the region of pure Rayleigh scattering and domain-4 the region of Hanle effect (see Eqs. (A.11) and (A.12)). Except for the case of $\Theta = 0°$, the shape of domain-4 is not very sensitive to the value of the scattering angle Θ. The Hanle domain includes the line core. The redistribution function $R_{\rm II-AD}$ takes its largest value in the diagonal band along $x = x'$. Hence, for large values of x, the contribution of domain-4 to the scattering integral should be negligible. Thus we recover the standard behavior that the Hanle effect holds only in the line core $|x| < 3$.

We now turn to $R_{\rm III-AD}$. Domain-1 and domain-2 represent a weighted combination of isotropic and Hanle phase matrices (see Eqs. (A.8) and (A.9)). In domain-3 there is a combination of isotropic, Hanle and Rayleigh phase matrices (Eq. (A.10)). Thus in the line core, we have Hanle scattering with no Rayleigh contribution. For the wing frequencies, both Hanle and Rayleigh phase matrices contribute, weighted respectively by the factors $\beta^{(2)} - \alpha$ and α. For $R_{\rm III-AD}$ redistribution, which is somewhat similar to CRD, the maximum of the redistribution occurs for both x and x' in the line core. For x and x' large, we can assume $R_{\rm III-AD} = \phi(x)\phi(x')$, with ϕ the absorption coefficient. Hence, for large x, the main contribution to the scattering integral will come from domain-2, where Hanle scattering is present. Thus, in cases where both $R_{\rm II-AD}$ and $R_{\rm III-AD}$ contribute to the redistribution matrix, there will be some contribution to the Hanle effect, coming from domain-2 also. It should be larger than the corresponding contribution of domain-4, coming from $R_{\rm II-AD}$ since $R_{\rm II-AD}$ in domain-4 is smaller than $R_{\rm III-AD}$ in domain-2 as shown by the analytical expressions for $R_{\rm II-AD}$ and $R_{\rm III-AD}$.

We now consider the domains for the AA case which are shown in Fig. 2. The construction of the domains is explained in the Appendix Sect. A.2. First we remark that the structure is somewhat similar to the AD domains for a scattering angle of $\Theta = 90°$, except for a sharp narrowing of the diagonal stripe in the $R_{\rm II-AA}$ case. We note that AA domains are not simple averages of the AD domains shown in Fig. 1 (see [B97b]). All the discussions in Fig. 1, regarding the contributions of Hanle and Rayleigh scattering in the line core and wings, hold also for Fig. 2.

2.3. A typical Hanle PRD line transfer problem

In order to illustrate the transition from the Hanle dominated core to the Rayleigh dominated wing, we show, in Fig. 3, the Stokes Q and U parameters for pure Hanle scattering, pure Rayleigh scattering and the general case where both are considered. Such a comparison is carried out for both AA and AD cases. The method of solution of the transfer problem is described in Sect. 3. The parameter of the model are the same as in Figs. 4 to 7. They are given at the beginning of Sect. 3.3.

The general case of (H+R) clearly follows the Hanle type scattering in the line core ($|x| < 2.5$), and the Rayleigh scattering behavior in the wings ($|x| \geq 4.5$), for both Q and U. In the AA case, the Rayleigh type behavior for Q, starts even in the near wings ($|x| > 2.5$). We also note that, for both AA and AD, Stokes Q is bounded from above by the Rayleigh limit, and from below by Hanle limit. This is consistent with the fact that the Hanle effect decreases Stokes Q.

As for the U parameter, in the AA case, it follows the Hanle limit in the core and, in the wings, is smaller than the pure Hanle case, as expected. In the AD case, Stokes U also follows

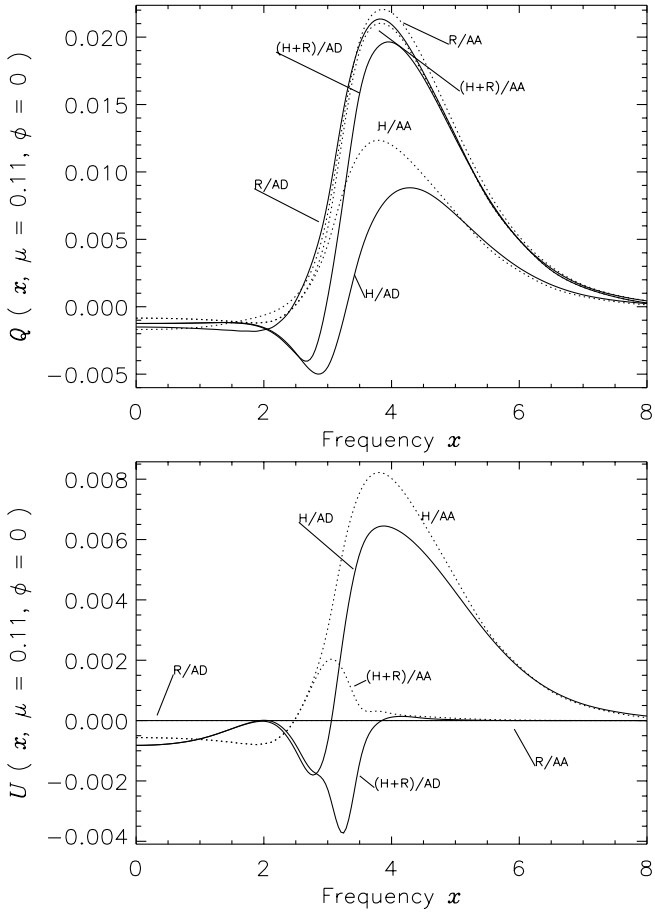

Fig. 3. The emergent Stokes Q and U profiles for pure Hanle (H), pure Rayleigh (R), and the general Hanle plus Rayleigh (H+R) scattering mechanisms. Dotted lines represent the AA redistribution, and the solid lines the corresponding AD redistribution. The exact frequency domains described in Figs. 1 and 2 are employed in these computations. Notice the smooth transition between the Hanle dominated line core and the Rayleigh dominated line wing. See Sect. 2.3 for more details.

the Hanle limit in the line core, but in the wings, there is a more complex behavior discussed in the forthcoming sections.

3. The numerical method of solution

It is possible to solve this line transfer problem by direct numerical schemes, such as the Feautrier method (Faurobert-Scholl 1994) or discrete space method (Nagendra 1988). But the memory and the CPU time requirements are very large. Here we use a simple perturbative approach.

3.1. The Generalized Perturbation Method (GPM)

Rees (1976) proposed a perturbation method for non-magnetic resonance scattering polarization. It is applicable when the degree of polarization of the radiation field is small, hence it is also applicable for the Hanle effect. The perturbative approach is quite simple. Here it is organized into three distinct stages. In stage 1 we solve a scalar PRD problem. In stage 2, we solve a polarization problem but consider the AA form of the redistribution function. Finally in stage 3 we solve the polarization problem with the AD redistribution function. In each stage, the solution is calculated iteratively.

In **stage 1** we solve a scalar transfer problem, with the line source function defined as:

$$S_{\ell,\mathrm{unpol}}(\tau,x) = \varepsilon B_{\nu_0} + \frac{1-\varepsilon}{\phi(\tau,x)} \int_{-\infty}^{+\infty} \mathrm{d}x' \frac{1}{2} \int_{-1}^{+1} \mathrm{d}\mu' \times \left[\gamma_{\mathrm{coh}} R_{\mathrm{II-AA}}(x,x') + (1-\gamma_{\mathrm{coh}}) R_{\mathrm{III-AA}}(x,x')\right] \times I(\tau,x',\mu'). \quad (5)$$

Here $\gamma_{\mathrm{coh}} = \alpha/(1-\varepsilon)$, with α defined in Eq. (A.14). The method of solution is a core-wing ALI iterative method with a short characteristic formal solver (FS) (Paletou & Auer 1995).

In **stage 2** we start the iteration cycle with the vector source function $\boldsymbol{\mathcal{S}}(\tau,x,\mu,\varphi) = [S(\tau,x),\ 0,\ 0]^{\mathrm{T}}$, where $S(\tau,x)$ is the solution of the scalar problem. The formal solution of the polarized transfer, calculated with a polarized FS (Nagendra et al. 1999), provides a Stokes vector which is incorporated into the AA version of Eq. (4) to obtain the next iterate of the source vector. The iteration is pursued until the convergence criterion is satisfied. At each step we calculate the Maximum Relative Change (MRC) in the degree of emergent linear polarization at the surface. We end the iteration when the MRC becomes less than a given value, say 10^{-2}.

In **stage 3** we proceed exactly as in stage 2. We start with the polarized source vector calculated in stage 2 using the AA redistribution function. After solving the transfer equation with the polarized FS, we use Eq. (4) to calculate the next iterate of the source vector. We apply the same convergence criterion as in stage 2.

Other computational details of the perturbative approach are described in Nagendra et al. (1999). In stage 2 we need the angle-averaged redistribution functions (see Eq. (A.3)). The integration over the scattering angle is performed numerically, using a Gauss-Legendre quadrature rule. The angle-averaged functions so computed give nearly the same emergent intensities as those obtained by the method of Adams et al. (1971), or the simpler approach of Gouttebroze (1986).

3.2. The memory and CPU time requirements of the Generalized Perturbation Method

An essential part of the perturbation method is the calculation of the scattering integral in Eq. (4). The scalar redistribution functions $R_{\mathrm{II-AD}}(x,x,\Theta)$ and $R_{\mathrm{III-AD}}(x,x',\Theta)$ which depend on the scattering angle $\Theta(\boldsymbol{n},\boldsymbol{n'})$ are given in Hummer (1962). Here we use respectively the Eqs. (59) and (61) in [B97b] to compute them. They differ by a constant factor with respect to the expressions given in Hummer (1962). Because of the symmetries of the redistribution functions under frequency exchange ($x \to x'$; and $x' \to x$), and with respect to the line center ($x \to -x$; and $x' \to -x'$), it suffices to solve the line transfer problem in a half-space in the outgoing frequency ($x > 0$). Hence we need to calculate the redistribution matrices only on the frequency range ($0 < x < +\infty$) and ($-\infty < x' < +\infty$). For a given value of x, the integration proceeds along a vertical line as shown for example in Fig. 1e. It is clear in this

figure that, for each value of x, $\boldsymbol{n}$, and $\boldsymbol{n}'$, one has to determine the boundaries of the domain 4. Thus for each set $(x; \boldsymbol{n}, \boldsymbol{n}')$, the values of x' corresponding to domain boundaries have to be determined. All these tests make the calculation of the scattering integral very expensive as far as computing time is concerned.

All the PALI methods that have been developed so far (with AA redistribution), make use of an azimuthal Fourier expansion of the Hanle phase matrix and of the Stokes vector. This decreases significantly, the memory requirement since one does not have to discretize over the azimuthal angle φ. The perturbation method developed here involves "explicit" numerical evaluation of the scattering integral through the quadrature sums on frequency (x), and the angles (μ and φ). Since the AD redistribution matrix exhibits strong variation with respect to the angles μ and φ, we need a grid-resolution of at least $N_\mu = 7$, and $N_\varphi = 16$ to obtain accurate results. This means 224 directions at every spatial and frequency point.

We have employed a non-uniform frequency grid consisting of $N_x = 41$ points. However the frequency variation of the AD redistribution function is so strong at certain scattering angles, that an ordinary grid with N_x points is not sufficient for an accurate frequency integration. The deficiency clearly shows up as low amplitude random oscillations of the Stokes Q and U, in the line core region. To circumvent this numerical problem, we have employed a linear spline (trapezoidal like) interpolation method to represent the strong frequency variation of the integrand. This procedure leads to a construction of, say, 6-point sub-division of each frequency interval Δx, and recomputing the "interpolated redistribution matrix weights" on a very fine frequency grid of $6N_x$ points. Notice that the transfer equation is still solved on the main nodes (N_x) of the frequency grid. For the above said reason, the perturbation code requires a large amount of CPU time to compute the AD redistribution matrices. It can be computed once and accessed later. Moreover if one wants to avoid wasting excessive computing time in repeated I/O operations, the polarized redistribution matrix has to be stored in the main memory. Depending on the grid resolution, this leads to a large demand on the computer memory also (4–40 GB for normal to good resolution!). For a real atmosphere one can follow the same procedure, but the redistribution weights have to be stored at all depths.

In the present code we have optimized the matrix multiplication $\hat{\mathcal{R}}\,\boldsymbol{I}$ in the integrand, by completely avoiding the random access in $(x, \boldsymbol{n}; x', \boldsymbol{n}'; I\,Q\,U)$ space inside nested do loops. This has been achieved by constructing and storing the redistribution matrix as an array suitable for 1D-ordered access. This speeds up the code by a factor of 5–10 compared to the conventional approach.

The requirements of memory and the CPU time to compute good solutions make the perturbation method a very demanding one. Computing time can be reduced by optimizing the code, and running on a parallel processor.

3.3. Parameterization of model atmosphere and the model atom

In this section we describe only those parameters, which are common to all the figures shown in this paper. All the results are presented for an isothermal and homogeneous slab. The atmospheric model parameters are $[T, a, \varepsilon, \beta, B_{\nu_0}]$, where T is the optical thickness of the slab. For Figs. 3 to 7 the model parameters are $[T, a, \varepsilon, \beta, B_{\nu_0}] = [2 \times 10^4, 10^{-3}, 10^{-3}, 0, 1]$. The slab is assumed to be self-emitting. There is no incident radiation on the boundaries. The magnetic field parameters are $[\Gamma_B, \theta_B, \varphi_B] = [1, 30°, 0°]$ unless stated otherwise. The magnetic field strength parameter Γ_B has a sensitivity range of $0.3 < \Gamma_B < 3$ for the Hanle effect. We have chosen $\Gamma_B = 1$ in all our numerical experiments. The magnetic field parameters are assumed to be independent of depth. The absorption profile is a Voigt function. The scalar redistribution functions that appear in the computation are of either AA-type, $R_{\rm II-AA}$ and $R_{\rm III-AA}$ or of AD-type, $R_{\rm II-AD}$ and $R_{\rm III-AD}$. The choice of collisional parameters is specific to each figure. Their values are given in the discussion concerning each figure. All the results in this paper are presented for $a = 10^{-3}$. The grid-resolution in physical variables is $[N_\tau, N_x, N_\mu, N_\varphi]$. The quantity N_τ represents the number of points per decade in a logarithmically spaced τ grid, with the first depth point $\tau_1 = 10^{-2}$. The frequency points are equally spaced in the line core, with a gradual switch over to logarithmic spacing in the wings, and satisfy $\phi(x_{\rm max})T \ll 1$ in the far wings. Unless stated otherwise, we used 6 points per decade for N_τ, $N_x = 41$, $N_\mu = 7$, and $N_\varphi = 16$.

3.4. The general characterization of collisions

There are different ways of studying the effects of collisional parameters in a parameterized manner (Domke & Hubeny 1988; Nagendra 1994, 1995). We have used the following approach:

i) Specify the thermalization parameter ε; strength of elastic collisions through Γ_E/Γ_R; the field strength through the parameter Γ_B, and the intrinsic de-polarization parameter $W_2 = 1$.

ii) Then compute the composite branching ratios α and $\beta^{(K)}$ using the Eqs. (A.14) and (A.15). The modified Hanle parameters Γ'' and Γ'_2 are given in Eq. (A.13).

We note here that the work of Bommier [B97b] has contributed to stabilize the definitions of the parameters Γ_B and of the branching ratios α and $\beta^{(2)}$.

In the case of pure coherent scattering (pure $R_{\rm II}$), the Hanle phase matrix involves the product $\alpha\Gamma_B$ (see Eqs. (A.11) and (A.13)). Here and in recent work ([B97b]; Faurobert-Scholl et al. 1999; Fluri et al. 2002), the denominator of $\alpha\Gamma_B$ is $\Gamma_R + \Gamma_I + \Gamma_E$. In Faurobert-Scholl (1993, 1994), this denominator is $\Gamma_R + D^{(2)}$, whereas it is $\Gamma_R + \Gamma_I + D^{(2)}$ in Bommier (1996), Faurobert-Scholl et al. (1997) and Nagendra et al. (1998). In stellar atmospheres, one has in general $\Gamma_I \ll \Gamma_E$ and $\Gamma_R \gg \Gamma_E$, hence the different choices of $\alpha\Gamma_B$ should lead to essentially the same surface polarization.

For a combination of coherent and incoherent scattering, it is the product $\beta^{(2)}\Gamma_B$ which controls the Hanle phase matrix at line center (see Eqs. (A.8), (A.11) and (A.13)), if we leave out the differences between $R_{\rm II}$ and $R_{\rm III}$ or consider quantities integrated over the line profile. The denominator of $\beta^{(2)}\Gamma_B$ is $\Gamma_R + \Gamma_I + D^{(2)}$.

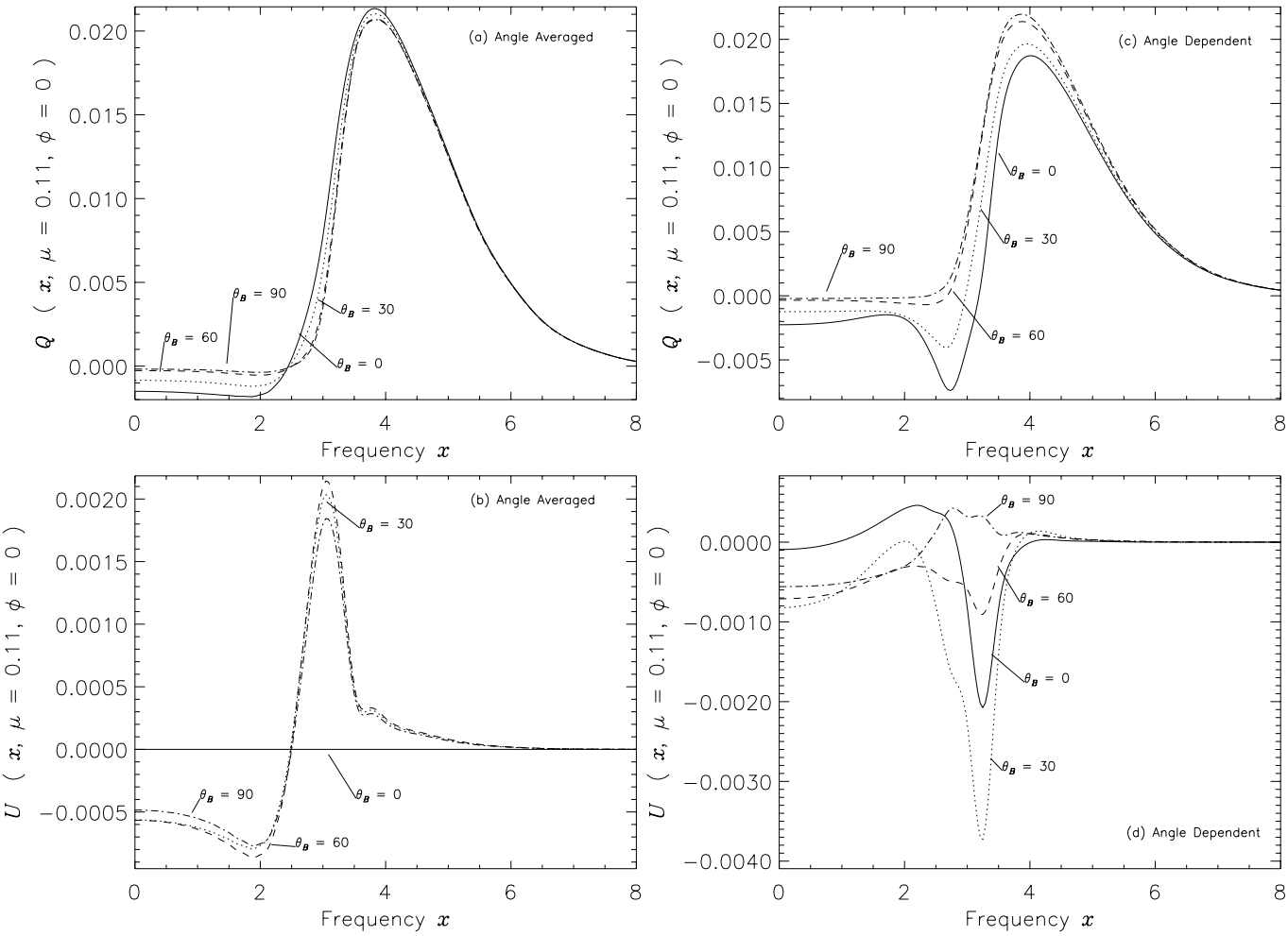

Fig. 4. The Hanle effect for different values of magnetic field inclination θ_B. The results are presented for the case of a pure R_{II} type redistribution (no elastic collisions). The curves are identified by the values of θ_B. Notice that AD approximation is more sensitive, than the AA approximation, to changes in θ_B. See Sect. 4.1 for more details.

4. Results and discussion

In this section, we present the results computed on the Hanle scattering problem with fully angle-dependent (AD) partial redistribution matrices. They are compared with the corresponding AA results. In the presence of an external magnetic field, the axi-symmetry of the diffuse radiation field about the vertical direction is lost. The atmospheric coordinate system in which the transfer equation is solved, consists of a z-axis (the normal to the planar slab), and the x-axis with respect to which the radiation field azimuthal angle (φ) and the magnetic field azimuth (φ_B) are measured (see Landi Degl'Innocenti & Landi Degl'Innocenti 1988; Frisch 1999). The polar angles of the radiation field and of the magnetic field are denoted θ and θ_B, respectively. In Sect. 4.1, we examine the θ_B dependence of Q and U and in Sect. 4.2, their dependence on φ.

The model atmosphere is described in Sect. 3.3. In Sects. 4.1 and 4.2 we are considering a pure R_{II} case. It corresponds to $\Gamma_E = D^{(2)} = 0$. Since $D^{(0)} = 0$, we have $\alpha = \beta^{(0)} = \beta^{(2)}$. We have chosen $\varepsilon = 10^{-3}$ which corresponds to $\alpha = 0.999$. Only the R_{II} related domains D4 and D5 become relevant. The associated polarization phase matrices are given in Eqs. (A.11) and (A.12). In Sect. 4.3, we consider the general case with elastic and de-polarization collisions ($\Gamma_E \neq 0$; $D^{(2)} \neq 0$).

4.1. A study of the Hanle effect for different field inclinations θ_B

In Fig. 4 we discuss the effect of varying θ_B on Q and U. The sensitivity of Q is small in the AA case but becomes significant in the AD case in the near wings. At line center, the sensitivity is about the same in the AA and AD cases. For a horizontal magnetic field ($\theta_B = 90°$) the AA and AD give about the same values of Q. The difference is maximum for $\theta_B = 0°$.

In the AA case, Stokes U is zero for $\theta_B = 0°$, due to symmetry, and departs from zero as soon as the field is non-vertical. Note also that, in the AA case the sensitivity o U to θ_B is not significant, at least in the range $30° < \theta_B < 90°$. In contrast, in the AD case Stokes U strongly depends on θ_B and we observe that $U \neq 0$ when the magnetic field is vertical ($\theta_B = 0°$), in contradiction to the expectation that $U = 0$ due to global symmetries. Accurate observations of the U profile, should make it possible to determine the orientation θ_B of the

magnetic field, provided the modeling is performed with an AD approximation.

The case of a vertical magnetic field has already been discussed in Frisch et al. (2001), and Faurobert et al. (2002). We summarize here the arguments presented in these references to explain that we may have $U \neq 0$ in the AD case. For simplicity, we consider the pure Hanle phase matrix in the scattering term in Eq. (3). The redistribution matrix then takes the form of a product

$$R\left(x, x', \mu, \mu', \varphi, \varphi'\right)\ \hat{P}_{\mathrm{H}}\left(\mu, \mu', \varphi, \varphi'; \theta_{\mathrm{B}}, \varphi_{\mathrm{B}}, \Gamma_{\mathrm{B}}\right), \tag{6}$$

where R can be any properly normalized scalar redistribution function. Both R and the phase matrix $\hat{P}_{\mathrm{H}}$ can be expanded in a Fourier series with respect to $(\varphi - \varphi')$.

Since the medium is axi-symmetric, we can assume that the incident radiation field is independent of φ'. In addition we assume for simplicity that it is unpolarized. Using the expression for $\hat{P}_{\mathrm{H}}$ corresponding to a vertical magnetic field (see Stenflo 1994, p. 89; and Frisch et al. 2001), we find that the scattering integral may be written

$$\boldsymbol{S}_{\mathrm{e}}(x, \mu) = \int_{-\infty}^{+\infty} \frac{1}{2} \int_{-1}^{+1} T\left(x, \mu, x', \mu'\right) \boldsymbol{S}_{\mathrm{i}}\left(x', \mu'\right)\ \mathrm{d}\mu'\ \mathrm{d}x', \tag{7}$$

where $\boldsymbol{S}_{\mathrm{e}}$ and $\boldsymbol{S}_{\mathrm{i}}$ are the emergent and incident Stokes vectors. Here

$$\begin{aligned}
\hat{T}\left(x, \mu, x', \mu'\right) \ =\ & R_0\left(x, \mu, x', \mu'\right) \hat{P}_0\left(\mu, \mu'\right) \\
+\ & \frac{3}{4} R_1\left(x, \mu, x', \mu'\right) \cos\alpha_1 \sin\theta \sin\theta' \\
\times\ & \left[\cos\alpha_1\, \hat{P}_1^2\left(\mu, \mu'\right) - \sin\alpha_1\, \hat{P}_{-1}^2\left(\mu, \mu'\right)\right] \\
+\ & \frac{3}{8} R_2\left(x, \mu, x', \mu'\right) \cos\alpha_2 \\
\times\ & \left[\cos\alpha_2\, \hat{P}_2^2\left(\mu, \mu'\right) - \sin\alpha_2\, \hat{P}_{-2}^2\left(\mu, \mu'\right)\right].
\end{aligned} \tag{8}$$

R_0, R_1 and R_2 are the coefficients of order zero, one and two in the Fourier azimuthal expansion of the redistribution function. In the AA case, R_1 and R_2 are zero. The coefficients α_1 and α_2 depend only on the magnitude of the magnetic field. The matrix $\hat{P}_0$ is the Rayleigh phase matrix. The matrices $\hat{P}_{\pm 1}^2$ and $\hat{P}_{\pm 2}^2$ can be found in Stenflo (1994 pp. 88, 89). In $\hat{P}_{-1}^2$ and $\hat{P}_{-2}^2$, the elements (3, 1) which couple U to I are different from zero. Hence we find $U \neq 0$. The matrices $\hat{P}_{+1}^2$ and $\hat{P}_{+2}^2$ have elements which couple Q to I. They come as a small correction to the term arising from the Rayleigh phase matrix $\hat{P}_0$.

However, one recovers $U = 0$ when the radiation field is independent of frequency (see Frisch et al. 2001). The proof relies on the normalization of the redistribution function which can be written

$$\int_{-\infty}^{+\infty} R\left(x, x', \boldsymbol{n}, \boldsymbol{n}'\right)\ \mathrm{d}y = \phi\left(y'\right), \tag{9}$$

where ϕ represents the absorption profile and y and y' stand for x and x', or x' and x, respectively. This normalization holds for any redistribution function constructed by folding an atomic frame redistribution function with a Maxwellian velocity distribution (see Hummer 1962). In the general case of a frequency-dependent radiation field, we have

$$\int_{0}^{+\infty} U(x, \mu)\, \mathrm{d}x = 0, \tag{10}$$

for all values of μ. The proof relies on Eq. (9) with $y = x$. We have verified numerically that this property holds to a high accuracy (to 6th digit) if we employ an angular grid of 7 co-latitudes per half-space in θ, and 8 azimuth angles φ. Condition Eq. (10) can be used to check the numerical accuracy of radiative transfer codes incorporating the Hanle effect.

4.2. A study of the azimuthal anisotropy of the radiation

We concentrate on Q and U only, since I depends very weakly on the azimuth. The figures correspond to $\theta_{\mathrm{B}} = 30°$. For a vertical magnetic field, Q and U are independent of φ.

In Fig. 5 we show the emergent Q and U profiles calculated with the AA and AD redistribution functions for several values of φ. In Fig. 6, we show the same quantities as a function of φ for selected points in the frequency profile. In Fig. 5 we see that the azimuthal dependence appears mainly in the line center and near wings, i.e. in the frequency domain of the Hanle effect. We note also that this dependence is stronger in the AD case than in the AA case. This is particularly true for Stokes U. The magnitude of U is about 3 times larger in the AD case than in the AA case. This difference is due to the fact that we are properly keeping the angle-dependence in the redistribution function.

For a better understanding of the results presented in Figs. 5 and 6, we recall the Fourier azimuthal expansion of the vector source function $\boldsymbol{\mathcal{S}}$ given in Frisch (1999, Eqs. (25) and (26)) for complete frequency redistribution (CRD). The Stokes vector has a similar expansion (see Nagendra et al. 1998). For μ close to zero, we have,

$$\mathcal{S}_{\mathrm{Q}} \ \simeq\ \frac{3}{\sqrt{8}} S_{\mathrm{Q}} + \frac{\sqrt{3}}{2}\left(S_{+2} \cos 2\varphi - S_{-2} \sin 2\varphi\right) + O(\mu), \tag{11}$$

$$\mathcal{S}_{\mathrm{U}} \ \simeq\ \frac{\sqrt{3}}{2}\left(S_{-1} \cos\varphi - S_{+1} \sin\varphi\right) + O(\mu). \tag{12}$$

For CRD, the expansion coefficients S_{Q}, $S_{\pm 1}$ and $S_{\pm 2}$ are functions of τ only and for PRD, with angle-averaged redistribution functions, they are functions of τ and x. They depend on the magnetic field. We roughly have $|S_{\pm 2}| < |S_{\pm 1}| < |S_Q|$.

For the AA case, the results shown in Figs. 5 and 6 (panels a and b) can easily be interpreted with the help of Eqs. (11) and (12). Stokes Q is not very sensitive to φ because the φ-dependence appears only in the second order terms in the Fourier expansion. For U, we clearly see the 2π-periodicity (Fig. 6, panel b) and a close to exact symmetry about $U = 0$ (Fig. 5, panel b), which corresponds to $U(x, \mu, \pi + \varphi) \simeq -U(x, \mu, \varphi)$. As shown in Eq. (12), this symmetry would be exactly satisfied for $\mu = 0$. Note that it will hold for any direction of the magnetic field.

In the AD case, we observe that Q has a dependence on φ which is slightly larger than in the AA case (see Fig. 5) and a mixture of the first and second Fourier harmonics (see Fig. 6). For U we clearly see in Fig. 5 that the approximate symmetry with respect to $U = 0$ does not hold anymore. We note also for U a small negative φ-independent contribution. In Sect. 4.1 we have seen that there is a φ-independent term in U when the magnetic field is vertical. Preliminary calculations have been

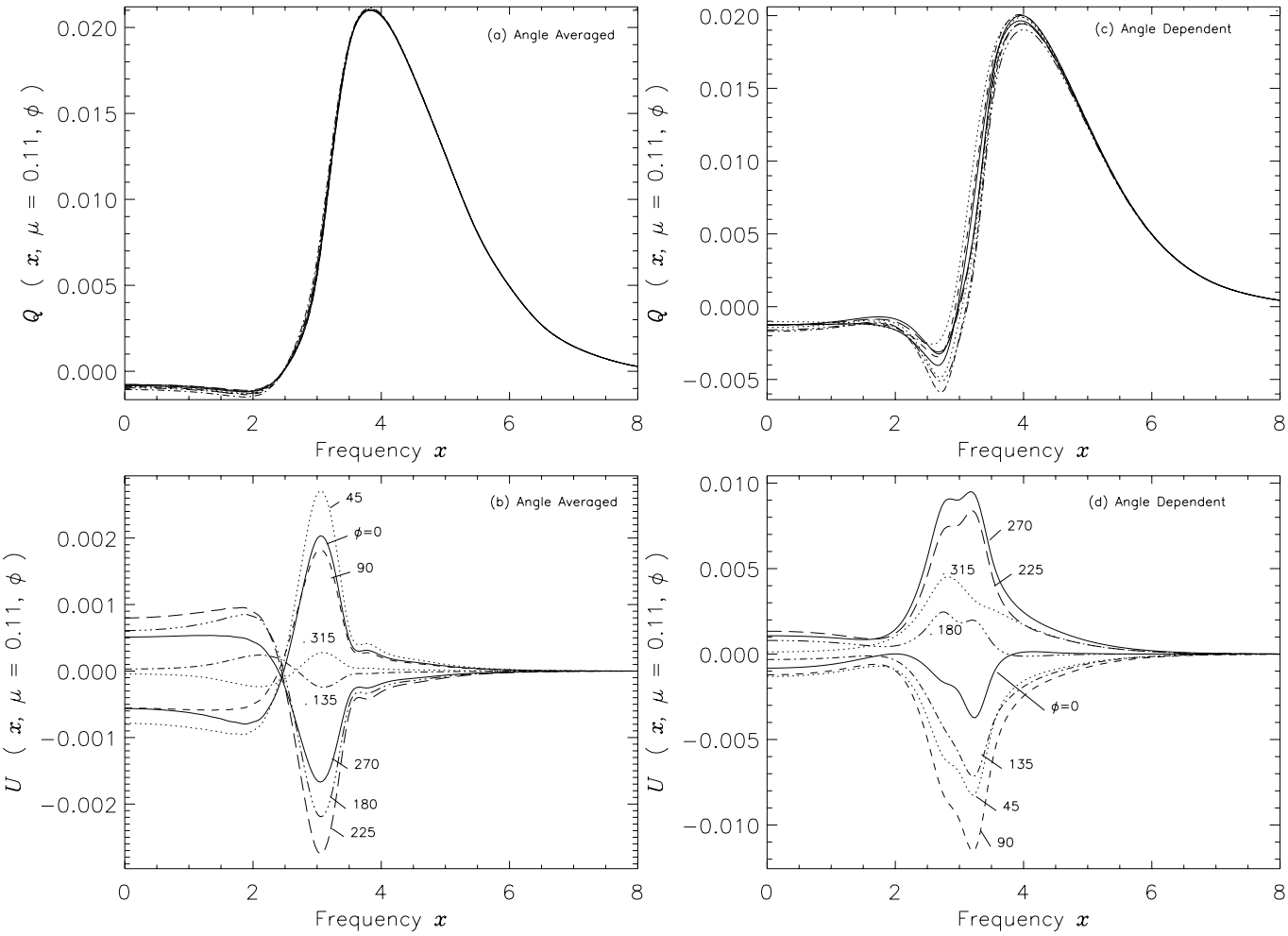

Fig. 5. The emergent Stokes Q and U profiles for several values of the radiation field azimuth φ. Same model parameters as for Fig. 4 are employed here. The curves are identified with the azimuth angle φ. The largest departures from axi-symmetry are around $x \approx v_c(a) \approx 3$. They are strong for U but remain very weak for Q. They appear mainly in the line core and near wings which are dominated by the Hanle effect. The large differences, in values and shape, between the AA and AD results, for Stokes U are discussed in Sect. 4.2.

performed for an arbitrary oriented magnetic field. The variations of Q and U with φ are still of the form given in Eqs. (11) and (12): in Stokes Q the φ-dependence is controlled at leading order by the second order Fourier component and in Stokes U by the first order one (the dominant Fourier component is the component of zeroth order, i.e. the one that does not depend depend on *varphi*). For U, there is an additional φ-independent term as for a vertical magnetic field.

4.3. The effect of elastic collisions on Hanle scattering polarization

In Fig. 7 we show the effect of elastic collisions and de-polarizing collisions on I, Q and U for the AA and AD cases. The redistribution matrix involves now contributions from both $R_{\rm II}$ and $R_{\rm III}$ type scattering. The AA case has already been explored by Faurobert-Scholl (1996 and references therein). The atmospheric model is the same as in Figs. 4 to 6. The differences are in terms of the branching ratio $\Gamma_{\rm E}/\Gamma_{\rm R}$, which takes the values $\Gamma_{\rm E}/\Gamma_{\rm R} = 0$, 0.1, 1, 10, 100. These 5 models are depicting a range, covering absence of elastic collisions, to the presence of very strong elastic collisions. Such a range of variation is indeed possible, in the solar atmosphere, as one goes down from the outermost shallow chromospheric layers to the base of the photosphere. For all the models $\varepsilon = 10^{-3}$ hence $\beta^{(0)} = 1 - \epsilon = 0.999$. For the de-polarizing collision rate we have $D^{(2)} = c\,\Gamma_{\rm E}$ with $c = 0.5$. The Voigt damping parameter a is kept at 10^{-3}. The variation of $\Gamma_{\rm E}/\Gamma_{\rm R}$ affects only the frequency redistribution and de-polarizing collisions.

Figure 7 shows that the I profiles become broader when the elastic collision rate is increased, while the line core is not modified. This is a standard result that can be understood in terms of Eq. (5). In the line core $R_{\rm III} \simeq R_{\rm II}$, hence there is no dependence on $\gamma_{\rm coh}$. In the wings, we go from the case of pure $R_{\rm II}$ type redistribution for $\Gamma_{\rm E}/\Gamma_{\rm R} = 0$ to a nearly pure $R_{\rm III}$ type redistribution for $\Gamma_{\rm E}/\Gamma_{\rm R} = 100$. We recall that $R_{\rm III}$ behaves essentially like complete frequency redistribution as soon as we are dealing with optically thick lines.

The polarization matrices, including elastic collisions, are defined in the Appendix. We give here simplified expressions of the redistribution matrix that would help us to understand the behaviors of Q and U. For simplicity we assume $\Gamma_2' = \Gamma''$

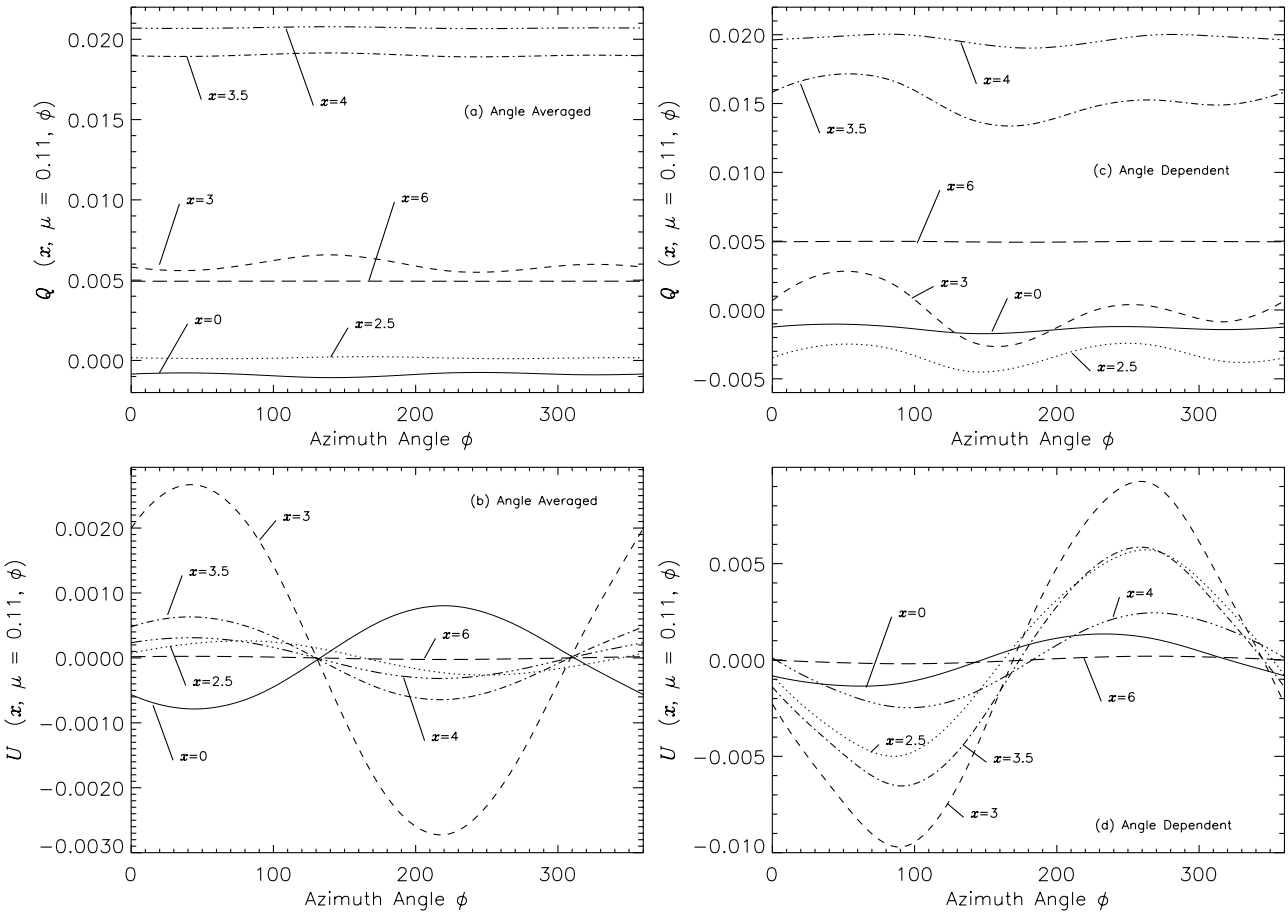

Fig. 6. The non-axi-symmetry of Stokes parameters at selected frequency points x in the line. The results are presented for the same model as that of Fig. 4. The curves are identified by the frequency points. Except for frequencies around $x = 3$, the Stokes Q parameter is axi-symmetric to a good accuracy. As expected, Hanle scattering strongly affects the Stokes U parameter in the AD case, which is artificially averaged out in the AA approximation. See Sect. 4.2 for more details.

(see Eq. (A.13)). The domains D1 and D2 have now the same polarization phase matrix, namely:

$$\hat{P}_{\rm III}({\rm D1, D2}) = \left(\beta^{(0)} - \beta^{(2)}\right)\hat{P}^{(0)} + \left(\beta^{(2)} - \alpha\right)\hat{P}_{\rm H}. \quad (13)$$

We recall that $\hat{P}^{(0)}$ is the isotropic phase matrix. In the line core, the relevant domains are D1 for $R_{\rm III}$ and D4 for $R_{\rm II}$ and we can assume $R_{\rm III} \simeq R_{\rm II}$. We thus find

$$\hat{\mathcal{R}}_{\rm core} \simeq \left[\left(\beta^{(0)} - \beta^{(2)}\right)\hat{P}^{(0)} + \beta^{(2)}\hat{P}_{\rm H}\right] R_{\rm II}. \quad (14)$$

In the line wings, the relevant domains are D2 for $R_{\rm III}$ and D5 for $R_{\rm II}$, hence

$$\hat{\mathcal{R}}_{\rm wing} \simeq \left(\beta^{(0)} - \beta^{(2)}\right)\hat{P}^{(0)}R_{\rm III} + \left(\beta^{(2)} - \alpha\right)\hat{P}_{\rm H}R_{\rm III} + \alpha\hat{P}_{\rm R}R_{\rm II}. \quad (15)$$

In Fig. 8, we show the variations of branching ratios α, $\beta^{(2)}$, $\beta^{(0)} - \beta^{(2)}$ and $\beta^{(2)} - \alpha$ as a function of $\Gamma_{\rm E}/\Gamma_{\rm R}$. All the parameters have a monotonic variation, except $\beta^{(2)} - \alpha$. It is easy to show that $\beta^{(2)} - \alpha$ has a maximum at $\Gamma_{\rm E}/\Gamma_{\rm R} = [(1-\epsilon)\sqrt{c}\,]^{-1}$. For our model, the maximum is at $\Gamma_{\rm E}/\Gamma_{\rm R} = 1.42$.

Panels b and e in Fig. 7 show that the sensitivity of Q to elastic collisions and de-polarizing collisions is essentially the same in the AA and the AD cases. We have already seen in previous sections that Q is not very sensitive to the coupling between frequency and angle redistribution. We observe in these panels a decrease in the polarization in the line core, a broadening of the wings, and in the wings, say for $|x| > 6$, a non-monotonic variation of Q which first increases with $\Gamma_{\rm E}/\Gamma_{\rm R}$ and then deceases when this ratio becomes larger than unity. In the line core, as shown by Eq. (14), the polarization is controlled by the parameter $D^{(2)}$, a property stressed in previous work (e.g. Nagendra 1994). Referring to Fig. 8, we see that $\beta^{(0)} - \beta^{(2)}$ increases while $\beta^{(2)}$ decreases when $\Gamma_{\rm E}/\Gamma_{\rm R}$ increases. Hence both terms in Eq. (14) contribute to decrease the polarization when the rate of de-polarizing collisions increases.

We now examine the wings of Q. Asymptotic analyses of radiative transfer for small values of ϵ (Frisch 1980) show that there is no isotropization of the radiation field in the line wings when they are formed under complete frequency redistribution or $R_{\rm III}$ partial redistribution. Since Q is a measure of the anisotropy of the radiation field, we can understand that Q increases in the wings together with the contribution of $R_{\rm III}$. In the wings, loosely speaking, $R_{\rm III}$ is larger than $R_{\rm II}$, hence the term with $R_{\rm III}$ in Eq. (15) will dominate over the term with $R_{\rm II}$, in spite of the fact that $(\beta^{(2)} - \alpha) < \alpha$ (see Fig. 8). The non-monotonic behavior of Q is thus a direct consequence of the non-monotonic variation of $\beta^{(2)} - \alpha$. The properties of Q discussed here do not depend in any critical way on the magnetic field. They should also hold for pure resonance scattering.

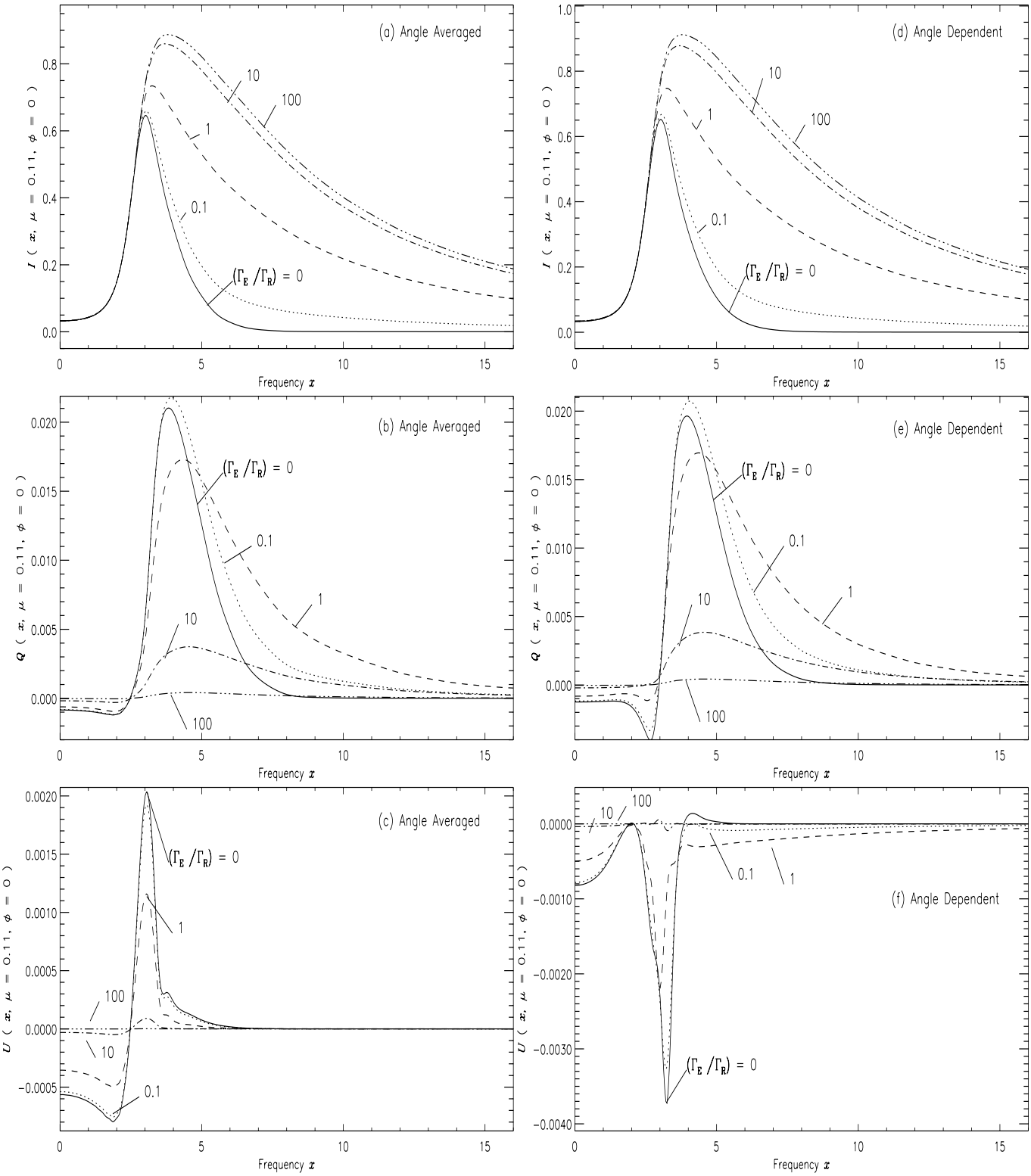

Fig. 7. Effect of elastic collisions on Hanle scattering polarization. The strength of collisions is characterized by the ratio (Γ_E/Γ_R), which take the values: 0, 0.1, 1, 10, 100. The curves are identified by this ratio. Notice that the Stokes U under the AD approximation is more sensitive to the elastic collisions, than under the AA approximation. See Sect. 4.3 for more details.

For Stokes U, in the AA case (panel c, Fig. 7), we observe a monotonic decrease of U at all wavelengths and no broadening of the profile. We have seen in Sect. 2.3 (see Fig. 3) that U reaches the Rayleigh limit $U = 0$ as soon as $|x| > 4.5$. This result was obtained for pure $R_{\rm II}$. The parameter U is a measure of departures from the axial symmetry. Increasing elastic collisions, i.e. going from an $R_{\rm II}$ redistribution to an $R_{\rm III}$ redistribution should have little effect on the azimuthal

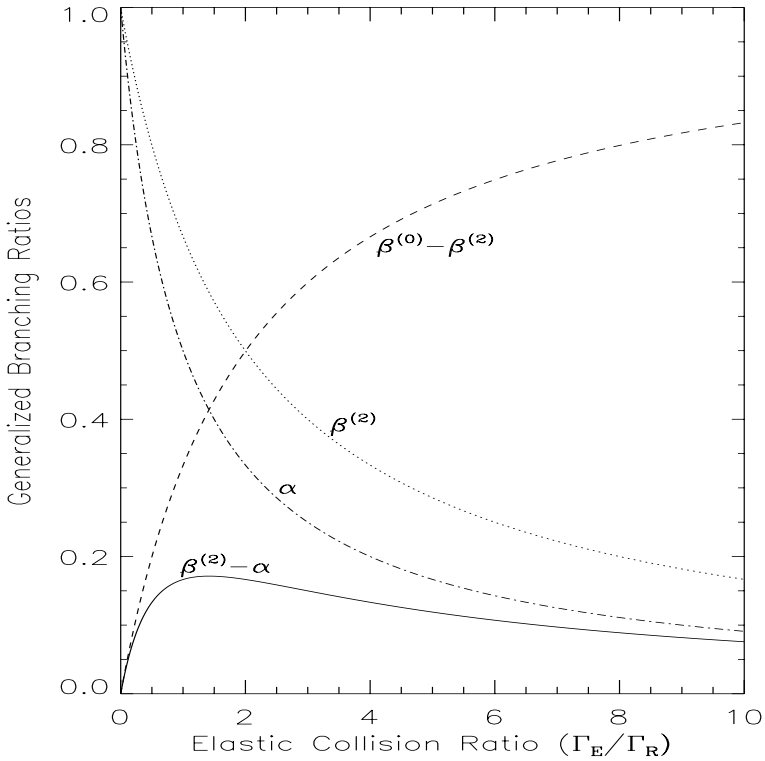

Fig. 8. Generalized branching ratios for Bommier's [B97b] domain based redistribution matrix. The dependence of these composite branching ratios on elastic collision rate is plotted. For $c = 0.5$ the quantity $\left(\beta^{(2)} - \alpha\right)$ asymptotically approaches α. Notice that, except for $\beta^{(2)} - \alpha$, other quantities show a monotonic variation with Γ_E/Γ_R. See Sect. 4.3 for details.

variation of the radiation field. Hence there should be no broadening of the U profile. It will remain in the region where the redistribution matrix can be approximated by Eq. (14). As seen above, both terms of this equation contribute to a decrease of the polarization when Γ_E/Γ_R increases.

In the AD case (panel f, Fig. 7), we observe a decrease of the polarization in the line core, which can be explained with Eq. (14). More interesting is the appearance of very low but extended wings where U varies in the same non-monotonic way as Q. We have seen in Figs. 4 to 6 that U has larger values in the AD case than in the AA case because of the φ-dependence of the redistribution function. This φ-dependence combined with the broadening of Stokes I can explain the formation of wings in the U profile. The non-monotonic variation of U is the signature of the magnetic field acting through the second term in Eq. (15). For a vertical magnetic field, we should observe similar extended wings in U.

A magnetic field effect has been detected recently by Bianda et al. (2002) in the wings of the U profile of the Ca I 4227 Å line. Whether this observation can be understood in terms of the Hanle effect needs a realistic modeling including an angle-dependent partial redistribution function.

4.4. The case of Hanle PRD scattering in an effectively thin slab

We have also considered a slab with an optical thickness T of only 200, which is effectively thin, which means that the radiation field does not thermalize at the slab center. We refer to this model as the thin slab. The full characteristics of the model are $[T, a, \varepsilon, \beta, B_{\nu_0}] = [200,\ 10^{-3},\ 10^{-3},\ 0,\ 1]$. We consider the pure $R_{\rm II}$ case with $\alpha = \beta^{(0)} = \beta^{(2)} = 0.999$. The magnetic field is defined by $\Gamma_B = 1.0$, $\theta_B = 30°$ and $\varphi_B = 0°$. The medium is assumed to be isothermal and self emitting. The grid resolution is: $N_d = 41$ (5 points/decade); $N_\mu = 7$; $N_\varphi = 8$; $N_x = 39$.

In Fig. 9 we show I, Q, and U for AA and AD redistribution cases. It can be seen in Fig. 9b that there is large difference in the Q profile depending on whether we employ AA or AD redistribution functions. This difference is considerably smaller for the effectively thick slab, as can be seen for instance in Fig. 5. In the thin slab case, in contrast to the effectively thick case, the radiation field does not become isotropic at large optical depths. This is the reason why using an AA redistribution is highly inadequate. We remark also that the ratio (Q/I) for the thin slab case is smaller than in the thick slab case (compare with Fig. 7). This ratio is controlled by the limb darkening of the I parameter, which is much smaller for a thin slab, than a thick slab.

For Stokes U, we see the same kind of difference between the AA case and the AD case as for an effectively thick slab (see Fig. 4). Contrary to Q, the ratio (U/I) has similar value in the thin and thick slab cases. This is because Stokes U is mainly controlled by the breaking of the axi-symmetry of Stokes I.

4.4.1. Comparison of exact and simple domains for the Hanle PRD problem

We have seen in the preceding sections that the Hanle effect is active mainly in the line core and the Rayleigh effect in the line

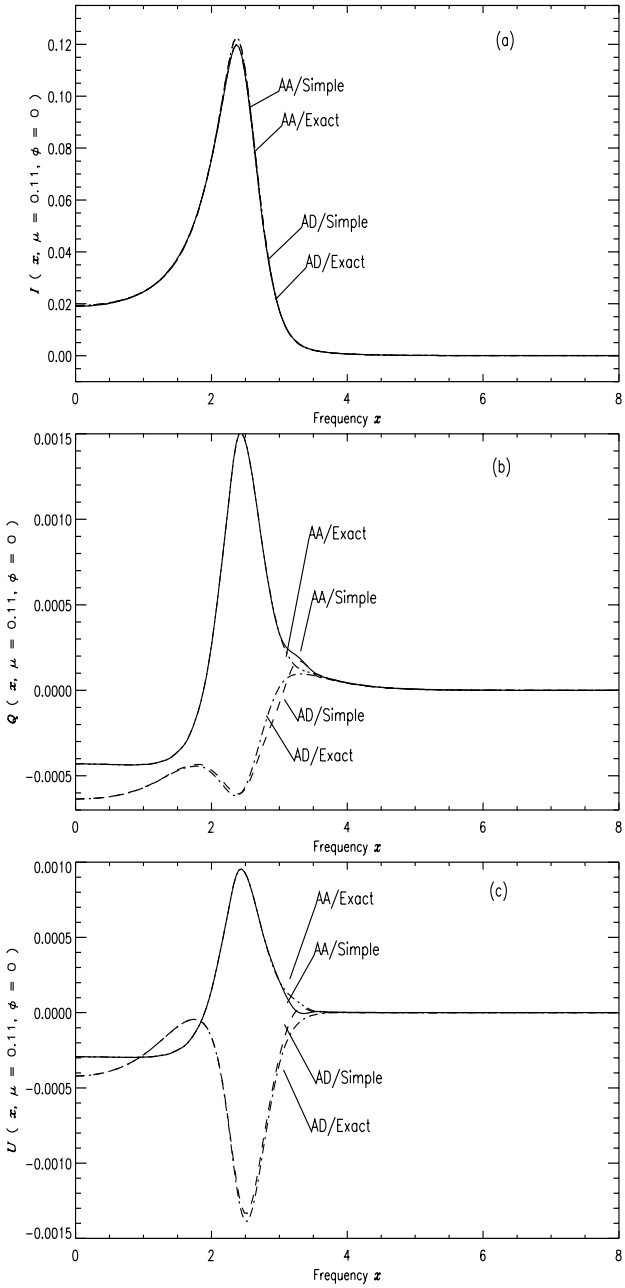

Fig. 9. The thin slab case. Comparison of simple and exact domains in the Hanle PRD problem. The simple domain refers to the vertical stripe, while exact domain means the use of the domains shown in Figs. 1 and 2 for the AD and AA cases, respectively. Notice that the use of a simple domain is sufficiently accurate in the computation of polarized emergent line profiles. See Sect. 4.4 for more details.

wings. This has lead to a standard cut-off approximation, which we refer to as the vertical stripe approximation. It is assumed that the Hanle effect acts only for $|x| < x_{\rm Hanle}$ and the Rayleigh effect for $|x| > x_{\rm Hanle}$, with $x_{\rm Hanle}$ given a priori. In this section we compare the emergent Stokes vector calculated with the method described in this paper and with the vertical stripe approximation, for the thin slab case. In the thin slab model (see Sect. 4.4), we have assumed a pure $R_{\rm II}$ frequency redistribution. Hence, the approximation amounts to replace the domain D4 by a vertical stripe. This means that we are neglecting the Hanle effect in the wings and thus we expect $|Q_{\rm exact}| < |Q_{\rm approx}|$, and $|U_{\rm exact}| > |U_{\rm approx}|$.

We have seen in Sect. 2 that a physically meaningful cut-off frequency is $x_{\rm Hanle} \simeq v_{\rm c}(a)$, with $v_{\rm c}(a)$ the transition frequency between the Gaussian core and the Lorentzian wings in the absorption profile. In Fig. 9 we compare the Stokes profiles calculated with the true domain D4 and the approximate one. We observe that the vertical stripe approximation underestimates the Hanle effect, as predicted. This conclusion holds for the AD and the AA case, with the effect being slightly larger in the AD case. For a mixture of $R_{\rm II}$ and $R_{\rm III}$, the under-estimation could be more pronounced because the vertical stripe approximation also neglects the contribution of the domain D2 to the Hanle effect.

Hence we suggest that in a preliminary modeling work, the vertical stripe approximation is good enough. The same conclusion was reached in Faurobert et al. (1999). For the cut-off frequency, $x_{\rm Hanle} = v_{\rm c}(a)$ should be preferred to a fixed value, say $x_{\rm Hanle} = 3.5$.

5. Conclusions

In this paper we have solved the problem of Hanle effect with PRD, using the theory developed by Bommier (1997b). This theory identified two levels of approximation, involving respectively AA and AD scalar redistribution functions. The coupling between frequency redistribution and angular redistribution is properly taken into account, when one uses the AD redistribution function. This coupling is ignored when working with AA redistribution function.

For lines with very large optical thickness (strong resonance lines), the Q parameter is fairly well represented by the angle-averaged approximation. In contrast, very large differences between angle-averaged and angle-dependent approximations exist in the emergent Stokes U parameter. Hence this coupling is definitely to be taken into account for accurate modeling of the Stokes U parameter, and subsequent determination of the magnetic field orientation. We have noticed an interesting effect of elastic collisions which can produce extended wings in the Stokes U parameter when $\Gamma_{\rm E}/\Gamma_{\rm R} \simeq 1$. These wings show up only with the AD redistribution functions and seem to be a signature of the Hanle effect. As pointed out in Bianda et al. (2002), the mechanism could be radiative excitation in the line core followed by a collision shift at a wing frequency, without destruction of the atomic polarization.

For weak lines, both Q and U parameters are very sensitive to the coupling between frequency and angular redistribution.

Our calculations have been carried out using the idea of "combined frequency domains" proposed in Bommier (1997b). Each domain refers to a given redistribution mechanism ($R_{\rm II}$ or $R_{\rm III}$), and to a polarization mechanism which is a combination of Rayleigh and Hanle scattering. We have also carried out some calculations with a simple domain decomposition, where the Hanle effect holds only in the line core, and Rayleigh scattering holds in the wings. It is found that the latter is a very good approximation. Thus, one feels confident that the use of such simple domains is sufficient in the radiative transfer analysis of polarimetric data.

Our calculations have clearly shown that it is necessary to make simultaneous measurements of Q and U with high polarimetric sensitivity (up to 10^{-4}) if one wants to properly determine the orientation of weak magnetic fields in the solar atmosphere. Measuring Stokes U with a high accuracy is also necessary to distinguish between an oriented or a microturbulent magnetic field (randomly oriented on scales smaller than typical photon mean free paths). The signature of a microturbulent field is a Stokes Q smaller than predicted on the basis of resonance scattering and a zero Stokes U. For a microturbulent magnetic field, the redistribution matrix can be averaged over the random orientations of the magnetic field and one is left with a resonance scattering problem with a renormalized de-polarization parameter which incorporates the effect of the magnetic field (Stenflo 1994). For resonance scattering, as shown in Faurobert (1987, 1988), the effects of angular dependence in the frequency redistribution function are quite small.

Acknowledgements. K. N. Nagendra is grateful to the scientists and other staff at the Observatoire de la Côte d'Azur (OCA), Nice, France for their warm hospitality during his visits to OCA. He is grateful to Dr. Baba Varghese for help with graphics. The authors like to thank Dr. J. P. Rivet and Mr. J. M. Mercier for arranging special provisions at the SIVAM computing facilities which enabled them to run the transfer code with finer grids. Hélène Frisch would like to thank the Indo-French Scientific Collaborative Programme CEFIPRA (2404-2), for partial support in organizing a visit to Indian Institute of Astrophysics (IIA), Bangalore, and also the Director of IIA for providing the local support. The authors are grateful to Dr. V. Bommier for useful discussions and for providing a highly accurate code to compute $R_{\rm III}$ functions. They have greatly benefited from remarks of the referee, who is heartily thanked.

Appendix A: The frequency domains and polarization phase matrices

For the convenience of the reader, we recall here the definitions of the frequency domains and of the polarization phase matrices that have been introduced in [B97b]. We write the latter in a slightly different form.

A.1. The angle-dependent frequency domains

The domains for $R_{\rm III-AD}$ can be defined as follows:

If $\{|x' - x\cos\Theta| < v_{\rm c}(a/\sin\Theta)\ \sin\Theta$
and $|x| < v_{\rm c}(a)|\cos\Theta| + v_{\rm c}(a/\sin\Theta)\ \sin\Theta$
and $|x - x'\cos\Theta| < v_{\rm c}(a/\sin\Theta)\ \sin\Theta$
and $|x'| < v_{\rm c}(a)|\cos\Theta| + v_{\rm c}(a/\sin\Theta)\ \sin\Theta\}$
then: **Domain** D1
else, if $\{|x| < v_{\rm c}(a)$ or $|x'| < v_{\rm c}(a)\}$
then: **Domain** D2
else: **Domain** D3
endif. (A.1)

The structure of the angle-dependent domains for $R_{\rm II-AD}$ are as follows:

If $\{|x + x'| < 2v_{\rm c}(a/\cos(\Theta/2))\ \cos(\Theta/2)\}$
then: **Domain** D4
else: **Domain** D5
endif. (A.2)

These relations involve a function $v_{\rm c}$. For a Voigt function of damping parameter a, $v_{\rm c}(a)$ is the frequency at which the Gaussian core becomes equal to a Lorentzian with parameter a (see [B97b] Eq. (85)). The values of a which appear in the definition of the domains can be understood by considering the analytical expression of the AD redistribution functions (Mihalas 1978; [B97b]).

A.2. The angle-averaged domains

The angle-averaged redistribution functions are defined as follows:

$$R_{\rm AA}(x, x') = \frac{1}{2}\int_0^{\pi} R_{\rm AD}(x, x', \Theta)\sin\Theta\,{\rm d}\Theta. \quad (A.3)$$

Angle-averaging the exact redistribution matrix as in Eq. (A.3), Bommier [B97b] has constructed frequency domains for the Level-III approximation. With $z = 2\sqrt{2} + 2$, the definitions of the $R_{\rm III-AA}$ domains may be written as:

If $\{zv_{\rm c}(a)|x'| - (x^2 + x'^2) < (z-1)v_{\rm c}^2(a)$
and $zv_{\rm c}(a)|x| - (x^2 + x'^2) < (z-1)v_{\rm c}^2(a)$
and $|x'| < \sqrt{2}v_{\rm c}(a)$
and $|x| < \sqrt{2}v_{\rm c}(a)\}$
then: **Domain** D1
else, if $\{|x| < v_{\rm c}(a)$ or $|x'| < v_{\rm c}(a)\}$
then: **Domain** D2
else: **Domain** D3
endif. (A.4)

The structure of the domains for $R_{\rm II-AA}$ are as follows:

If $\{x(x + x') < 2v_{\rm c}^2(a)$
and $x'(x + x') < 2v_{\rm c}^2(a)\}$
then: **Domain** D4
else: **Domain** D5
endif. (A.5)

A.3. The polarization phase matrices

For a two-level atom, the Rayleigh and Hanle phase matrices can be written in terms of a multi-polar expansion of the form

$$\hat{P}(\boldsymbol{n}, \boldsymbol{n'}) = \sum_{K=0}^{K=2} W^{(K)}(J, J')\,\hat{P}^{(K)}(\boldsymbol{n}, \boldsymbol{n'}), \quad (A.6)$$

with $W^{(K)}(J, J')$ the de-polarization parameter(see e.g. Eq. (26) of [B97b]; Landi Degl' Innocenti 1984). The term with $K = 1$

corresponds to circular polarization which is not considered in this paper. Here we consider a normal Zeeman triplet $J = 0$, $J' = 1$. Hence the $W^{(K)}$ are equal to unity. The zeroth-order term $\hat{P}^{(0)}$ is the isotropic scattering phase matrix (the element (1,1) is unity and the others are zero).

The analytical expression of the Hanle Phase matrix $\hat{P}_{\rm H}$ is given in Landi Degl' Innocenti & Landi Degl' Innocenti (1988) for an arbitrary reference frame. It depends on the orientation of the magnetic field, $\boldsymbol{n}_{\rm B}$, and on the non-dimensional magnetic field strength parameter

$$\Gamma_{\rm B} = g_{J'}\frac{\omega_{\rm L}}{\Gamma_{\rm R}}; \quad \text{with} \quad \omega_{\rm L} = \frac{eB}{2m_{\rm e}c}. \tag{A.7}$$

The quantity $g_{J'}$ is the Landé factor of the upper level and $\omega_{\rm L}$ the Larmor frequency.

The polarization phase matrices introduced in Eq. (4) are common to the AA and AD cases. In [B97b] they are defined in terms of $\hat{P}^{(0)}$, $\hat{P}^{(2)}_{\rm R}$ and $\hat{P}^{(2)}_{\rm H}$. Here they are expressed in terms of the full matrices $\hat{P}_{\rm R}$ and $\hat{P}_{\rm H}$. For the domains D1 to D5, we have

$$\begin{aligned}\hat{P}_{\rm III}({\rm D1}) &= \left(\beta^{(0)} - \beta^{(2)}\right)\hat{P}^{(0)} \\ &+ \beta^{(2)}\hat{P}_{\rm H}\left(\boldsymbol{n},\boldsymbol{n}';\boldsymbol{n}_{\rm B},\Gamma'_2\right) - \alpha\hat{P}_{\rm H}\left(\boldsymbol{n},\boldsymbol{n}';\boldsymbol{n}_{\rm B},\Gamma''\right),\end{aligned} \tag{A.8}$$

$$\hat{P}_{\rm III}({\rm D2}) = \left(\beta^{(0)}-\beta^{(2)}\right)\hat{P}^{(0)}+\left(\beta^{(2)}-\alpha\right)\hat{P}_{\rm H}\left(\boldsymbol{n},\boldsymbol{n}';\boldsymbol{n}_{\rm B},\Gamma'_2\right), \tag{A.9}$$

$$\begin{aligned}\hat{P}_{\rm III}({\rm D3}) &= \left(\beta^{(0)} - \beta^{(2)}\right)\hat{P}^{(0)}+\frac{\beta^{(2)}-\alpha}{\beta^{(2)}} \\ &\times\left[\left(\beta^{(2)}-\alpha\right)\hat{P}_{\rm H}\left(\boldsymbol{n},\boldsymbol{n}';\boldsymbol{n}_{\rm B},\Gamma'_2\right)+\alpha\hat{P}_{\rm R}\left(\boldsymbol{n},\boldsymbol{n}'\right)\right],\end{aligned} \tag{A.10}$$

$$\hat{P}_{\rm II}({\rm D4}) = \alpha\hat{P}_{\rm H}\left(\boldsymbol{n},\boldsymbol{n}';\boldsymbol{n}_{\rm B},\Gamma''\right), \tag{A.11}$$

$$\hat{P}_{\rm II}({\rm D5}) = \alpha\hat{P}_{\rm R}(\boldsymbol{n},\boldsymbol{n}'). \tag{A.12}$$

The collisional rates Γ'_K and Γ'' are given by

$$\Gamma'_2 = \beta^{(2)}\Gamma_{\rm B}; \quad \text{and} \quad \Gamma'' = \alpha\Gamma_{\rm B}, \tag{A.13}$$

where α and $\beta^{(2)}$ are the collisional branching ratios introduced below.

A.4. The collisional redistribution branching ratios

Following [B97b] we employ branching ratios defined as:

$$\alpha = \frac{\Gamma_{\rm R}}{\Gamma_{\rm R}+\Gamma_{\rm I}+\Gamma_{\rm E}}, \tag{A.14}$$

$$\beta^{(K)} = \frac{\Gamma_{\rm R}}{\Gamma_{\rm R}+\Gamma_{\rm I}+D^{(K)}}, \tag{A.15}$$

where $K = 0$ or 2. The quantity $\Gamma_{\rm R}$ is the radiative de-excitation rate (natural width of the upper level), and $\Gamma_{\rm I}$ is the rate of inelastic collisions between radiating and perturbing atoms which causes destruction of the upper excited level. The total rate of elastic collisions $\Gamma_{\rm E}$ causes collisional broadening of the upper level and destruction of photon correlations in the atomic frame. They produce large non-coherence in frequency in atomic and hence also in the laboratory frame. All types of elastic collisions are included in $\Gamma_{\rm E}$. In astrophysical plasma, the major source of perturbation are neutral hydrogen atoms. The quantity $D^{(K)}$ are the K-multi-pole de-polarizing collision rates. For $K = 0$, we have $D^{(0)} = 0$, and $D^{(2)}$ is a simple function of $\Gamma_{\rm E}$, such as

$$D^{(2)} = c\,\Gamma_{\rm E}, \quad 0 \le c \le 1. \tag{A.16}$$

The $D^{(K)}$ are most effective causes of decreasing the linear polarization in spectral lines, because they destroy the atomic alignment. In the computations presented in this paper, we have employed $c = 0.5$. We note that the branching ratio $(\beta^{(2)} - \alpha)$ which multiplies the Hanle phase matrix in Eqs. (A.9) and (A.10) corresponds to elastic collisions which do not destroy the alignment.

The parameter ε in Eq. (3) is given by

$$\varepsilon = \frac{\Gamma_{\rm I}}{\Gamma_{\rm R}+\Gamma_{\rm I}}. \tag{A.17}$$

In the definition of ε we have neglected stimulated emission. The Voigt damping parameter a is defined through the relation

$$a = \frac{\Gamma_{\rm R}+\Gamma_{\rm E}}{4\pi\Delta\nu_{\rm D}}, \quad \text{where} \quad \Delta\nu_{\rm D} = \frac{\nu_0}{c}\sqrt{\frac{2kT_{\rm e}}{M_a}}. \tag{A.18}$$

References

Adams, T. F., Hummer, D. G., & Rybicki, G. B. 1971, J. Quant. Spectrosc. Radiat. Transfer, 11, 1365

Bianda, M., Stenflo, J. O., Gandorfer, A., & Gisler, D. 2002, in Current Theoretical models and Future High Resolution Observations: preparing for ATST, ed. A. A. Pevtsov, & H. Uitenbroek, ASP Conf. Ser., in press

Bommier, V. 1996, Sol. Phys., 164, 29

Bommier, V. 1997a, A&A, 328, 706 [B97a]

Bommier, V. 1997b, A&A, 328, 726 [B97b]

Bommier, V., & Stenflo, J. O. 1999, A&A, 350, 327

Domke, H., & Hubeny, I. 1988, ApJ, 334, 527

Faurobert, M. 1987, A&A, 178, 269

Faurobert, M. 1988, A&A, 194, 268

Faurobert-Scholl, M. 1993, A&A, 268, 765

Faurobert-Scholl, M. 1994, A&A, 285, 655

Faurobert-Scholl, M. 1996, in Solar Polarization, ed. J. O. Stenflo, & K. N. Nagendra (Kluwer Academic Publishers), 79 (also Sol. Phys., 164, 79)

Faurobert-Scholl, M., Frisch, H., & Nagendra, K. N. 1997, A&A, 322, 896

Faurobert-Scholl, M., Paletou, F., & Bommier, V. 1999, in ASSL 243, Solar Polarization, ed. K. N. Nagendra, & J. O. Stenflo (Kluwer Academic Publishers), 115

Faurobert, M., Frisch, H., & Nagendra, K. N. 2002, in Magnetic Fields across the HR diagram, ed. G. Mathys, S. Solanki, & D. T. Wickramasinghe, ASP Conf. Ser., 248, 145

Fluri, D. M., Nagendra, K. N., & Frisch, H. 2002, A&A, submitted

Frisch, H. 1980, A&A, 83, 166

Frisch, H. 1999, in ASSL 243, Solar Polarization, ed. K. N. Nagendra, & J. O. Stenflo (Kluwer Academic Publishers), 97

Frisch, H., Faurobert, M., & Nagendra, K. N. 2001, in Advanced Solar Polarimetry: Theory, Observation and Instrumentation, ed. M. Sigwarth, ASP Conf. Ser., 236, 197

Gouttebroze, P. 1986, A&A, 160, 195

Hummer, D. G. 1962, MNRAS, 125, 21

Landi Degl'Innocenti, E. 1983, Sol. Phys., 85, 3

Landi Degl'Innocenti, E. 1984, Sol. Phys., 91, 1
Landi Degl'Innocenti, E. 1985, Sol. Phys., 102, 1
Landi Degl'Innocenti, M., & Landi Degl'Innocenti, E. 1988, A&A, 192, 374
Landi Degl'Innocenti, E., Landi Degl'Innocenti, M., & Landolfi, M. 1997, in Science with THEMIS, ed. N. Mein, & S. Sahal-Bréchot (Paris Observatory), 59
Mihalas, D. 1978, Stellar Atmospheres, 2nd edition (W. H. Freeman & Co., San Francisco)
Nagendra, K. N. 1988, ApJ, 335, 269
Nagendra, K. N. 1994, ApJ, 432, 274
Nagendra, K. N. 1995, MNRAS, 274, 523
Nagendra, K. N. 2002, in Stellar Atmosphere Modeling, ed. I. Hubeny, D. Mihalas, & K. Werner, ASP Conf. Ser., in press
Nagendra, K. N., & Frisch, H. 2003, in Proc. of the 3rd Solar Polarization Workshop (SPW3), preprint
Nagendra, K. N., Frisch, H., & Faurobert-Scholl, M. 1998, A&A, 332, 610
Nagendra, K. N., Paletou, F., Frisch, H., & Faurobert-Scholl, M. 1999, in ASSL 243, Solar Polarization, ed. K. N. Nagendra, & J. O. Stenflo (Kluwer Academic Publishers), 127
Nagendra, K. N., & Stenflo, J. O. 1999, ASSL 243, Solar Polarization (Kluwer Academic Publishers)
Omont, A., Smith, E. W., & Cooper, J. 1972, ApJ, 175, 185
Omont, A., Smith, E. W., & Cooper, J. 1973, ApJ, 182, 283
Paletou, F., & Auer, L. H. 1995, A&A, 297, 771
Rees, D. E. 1976, PASJ, 30, 455
Stenflo, J. O. 1994, Sol. Magnetic Fields (Kluwer Academic Publishers)
Stenflo, J. O., & Nagendra, K. N. 1996, Sol. Phys., 164
Trujillo Bueno, J. 2001, in Advanced Solar Polarimetry: Theory, Observation and Instrumentation, ed. M. Sigwarth, ASP Conf. Ser., 236, 161
Trujillo Bueno, J., Landi Degl'Innocenti, E., Collados, M., Merenda, L., & Manso Sainz, R. 2002, Nature, 415, 403